INDERSCIENCE PUBLISHERS
Linking academia, business and industry through research

International Journal of Nanotechnology

ISSN online: 1741-8151 - ISSN print: 1475-7435
https://www.inderscience.com/ijnt

Fishier mantis optimiser: a swarm intelligence algorithm for clustering images of COVID-19 pandemic

Javad Rahebi

DOI: 10.1504/IJNT.2021.10043394

Article History:

Received:	04 May 2021
Last revised:	07 July 2021
Accepted:	03 August 2021
Published online:	31 May 2023

Fishier mantis optimiser: a swarm intelligence algorithm for clustering images of COVID-19 pandemic

Javad Rahebi

Department of Software Engineering,
Istanbul Topkapi University,
Istanbul, Turkey
Email: cevatrahebi@topkapi.edu.tr

Abstract: In this study, an automated segmentation method is used to increase the speed of diagnosis and reduce the segmentation error of CT scans of the lung. In the proposed technique, the fishier mantis optimiser (FMO) algorithm is modelling and formulated based on the intelligent behaviour of mantis insects for hunting to create an intelligent algorithm for image segmentation. In the second phase of the proposed method, the proposed algorithm is used to cluster scanned image images of COVID-19 patients. Implementation of the proposed technique on CT scan images of patients shows that the similarity index of the proposed method is 98.36%, accuracy is 98.45%, and sensitivity is 98.37%. The proposed algorithm is more accurate in diagnosing COVID-19 patients than the falcon algorithm, the spotted hyena optimiser (SHO), the Grasshopper optimisation algorithm (GOA), the grey wolf optimisation algorithm (GWO), and the black widow optimisation algorithm (BWO).

Keywords: meta-heuristic algorithms; FMO; fishier mantis optimiser; COVID 19 disease; coronavirus; clustering.

Reference to this paper should be made as follows: Rahebi, J. (2023) 'Fishier mantis optimiser: a swarm intelligence algorithm for clustering images of COVID-19 pandemic', *Int. J. Nanotechnol.*, Vol. 20, Nos. 1/2/3/4, pp.25–49.

Biographical notes: Javad Rahebi is an Assistant Professor at the Faculty of Software Engineering, Istanbul Ayvansaray University, and teaches image processing, signal processing. His field of professional and scientific interest is image processing, optimisation methods, artificial intelligence, and deep learning. He is a keynote speaker and review member in some scientific journals. He authored several conference papers and many scientific papers in SCI, SCI-E, and SCOPUS journals. 1IEEE8023/Covid Chest X-Ray Dataset.

1 Introduction

At the end of 2019, the coronavirus began to spread in Hubei Province, China. COVID-19 disease has now spread to more than 200 countries around the world. COVID-19 is a newly recognised disease prevalent through the air and contact with infected objects and

people. COVID-19 became a pandemic in 2020 [1]. According to the World Health Organization (WHO), as of 30 June, 2020, more than 10 million cases of COVID-19 disease and more than half a million confirmed deaths. Infection of people with a type of SARS virus that attacks the lungs and respiratory system is the cause of COVID-19 disease [2]. Patients with COVID-19 disease may show symptoms of common flu, pneumonia, and other respiratory COVID-19 within the first four to 10 days [3].

To identify COVID-19 through computer-assisted diagnosis (CAD) is an essential diagnostic method to help patients. Image processing techniques used in computer-assisted diagnosis. Image processing is using computer-aided detection. By these methods, different parts of the body are scanning to diagnose the disease. A usual way for recognising the COVID-19 is the use of chest X-ray (CXR) images [4]. Computed tomography imaging techniques, as well as magnetic resonance imaging, are used to diagnose the disease, but X-ray imaging techniques are more common. Today, the most common imaging method for diagnosing COVID-19 in infected patients is the use of CT scans because they are more sensitive than chest X-rays [5]. Today, treatment resources are confining to many patients, and only patients with severe complications accept the hospital. A challenge is that CT scan units in hospitals are also limited. A person needs to have CT scans over several different periods to determine if the disease is spreading or improving. A challenge for physicians in diagnosing COVID-19 disease with CT scans is to confuse it with atypical pneumonia [6] and other pulmonary manifestations [7]. Pneumonia is an infectious disease that also affects the lung tissue. According to the World Health Organization, this disease is considering to be the leading cause of death in children. Pneumonia can be reason by a fungus, bacteria, or a virus attack on the lung tissue and damage it. Pneumonia causes chest pain and limits the amount of oxygen a patient can receive. Pneumonia shows radiological features such as fluid accumulation in the lungs. COVID-19 is a viral disease that causes a type of pneumonia. The cause of this disease is tissue damage in the immune system. COVID-19 disease causes fibrosis of the lungs, and CT scan images can show these areas in different colours [8].

One practical method in diagnosing COVID-19 disease is the use of CT scan images for segmenting in image processing. Clustering methods [9], neural network [10], deep learning [11], support vector machine [12], fuzzy methods [13], and swarm intelligence algorithms [14] are among the ways of automatic disease diagnosis COVID-19 based on lung CT scan image processing. Clustering is a simple yet effective way to diagnose COVID-19 based on CT scans. By clustering, the images are partitioned into different areas. Each area shows specific information from the image. Clustering is an unsupervised learning method and can be used to diagnose disease without training data. Traditional clustering methods such as Kmeans [15] and FCM [16], although widely used in segmenting, do not have high accuracy and do not perform clustering intelligently. The feature selection methods like FCBF [17] can use COVID-19 CT images to select the best features and use them in the deep learning methods.

A suitable method for clustering is the use of swarm intelligence methods to develop clustering methods. The behaviour of living things and phenomena that have an intelligent approach in nature can be impressive in creating a clustering method. One of the intelligent treatments for hunting, which has a high intelligence nature, is the behaviour of fishier mantis. Fishier mantis has an intelligent way of catching fish to find optimal cluster centers to reduce their output error in the segmentation area. The behaviour of the fishier mantis in this paper is the first structured. A meta-heuristic method is introduced based on it. In the second phase, the optimisation algorithm of

fishier mantis use for clustering and segmentation of CT scan images, fishier mantis disease. The contribution of this paper is to use the fishier mantis optimisation method for clustering the new COVID-19 disease.

In the first part of the paper, an introduction to the topic is introducing. Section 2 also discusses the background and related studies. In Section 3, the proposed method is introducing in two stages: meta-algorithm and image segmentation. In Section 4, the proposed method is implemented and analysed. In Section 5, the results of the implementation of the proposed technique and future work are suggested.

2 Related work

Coronavirus was notified of an epidemic by the World Health Organization. COVID-19 has infected more than 1 million people and killed more than 50,000. The clinical manifestations of COVID-19 disease are related to the time of exposure, the degree of exposure, the type of virus, etc. Most symptoms of COVID-19 occur as fever, chills, fatigue, occasional diarrhea, sore throat, or asymptomatic. Symptoms are mild in children and more severe in the elderly or patients with chronic underlying diseases. The presence of an infected person in the family causes infection and the spread of COVID-19 disease. Infection with COVID-19 disease causes pneumonia and be recognised by processing chest X-ray images. Many studies related to the diagnosis of COVID-19 use image processing and CT scan images of the lungs. Data mining, machine learning, and deep learning methods have a significant role in disease diagnosis. In the study [18], the automatic diagnosis of COVID-19 infection using chest X-ray images through transitional learning has been proposed. They proposed an auto-diagnostic method for COVID-19 based on chest X-ray images. The dataset for this study includes 194 X-ray images of patients with coronavirus and 194 X-ray images of healthy patients. Few images of COVID-19 disease are publicly available, so they provided transitional learning to meet this challenge. They used different convolution neural network architectures taught in ImageNet. In their proposed method, convolutional neural networks are hybridised with integrated machine learning methods such as multilayer neural networks and support vector machines. The results show that combining convolutional neural networks and multilayer artificial neural networks has the highest accuracy and is equal to 95.6%. In the study [19], chest X-ray imaging has been proposed using deep learning as a diagnostic tool for COVID-19 disease. Prompt detection of positive coronavirus cases prevents further spread of the population. Recent findings from chest X-rays and CT scans show a significant ability to detect the severity of the coronavirus in the lungs. Their proposed method for analysing chest X-ray images with a deep learning method for diagnosing the disease has good accuracy, but these methods require a lot of data and samples for training. In the study [20], artificial intelligence techniques for the diagnosis of COVID-19 are reviewed. Achieving artificial intelligence imaging can significantly help automate the scanning method of COVID-19 patients. Their proposed method minimises and protects patients from contact with imaging technicians. In this review paper, we review various aspects of the diagnosis of COVID-19 disease, including imaging, segmentations, diagnosis, etc. In the study [21], the findings of CT-Scan images of COVID-19 disease in families with common manifestations were examined. In the study [22], deep learning methods in medical imaging for diagnosing lung disease and the diagnosis of COVID-19 disease were

discussed. From February 2017 to May 2020, studies in diagnosing COVID-19 disease were reviewed by in-depth learning methods. In this paper, the diagnosis of COVID-19 disease has been surveyed using classification and zoning methods.

In the study [23], from artificial intelligence and deep learning, using CT scan images of the chest, they proposed a method of diagnosis and tracking of COVID-19 disease. In this paper, a 2D deep learning architecture with U-Net is as its backbone for the segmentation task. They evaluated their proposed method using public datasets available on GitHub and Kaggle. Experimental results show that the proposed method using U-Net architecture shows better results compared to the existing U-Net and U-net architecture. In the study [24], automatic quantification of the development of COVID-19 disease using chest CT scan images is presented. In this study, 120 CT scans images of people with damaged lungs were used for training deep learning algorithms. 72 scans of 24 patients were used to evaluate algorithms for diagnosing lung injury. Their algorithm had four steps: detecting the boundaries of the lungs and arteries, recording the edges of the lungs, identifying areas of pneumonitis, and assessing disease progression. Their experiments show that the proposed algorithm has a sensitivity of 95% and specificity of 84%.

Recently Computing QoS in medical Information system using Fuzzy (CQMISF) algorithm [25] and novel Intelligent Multimedia Data Segregation (IMDS) scheme [26] used fog computing [27] for medical information processing. In the CQMISF method, they used this method to transfer the classified high-risk data with an optimal gateway.

3 The proposed method

Most methods of diagnosing COVID-19 use deep learning and supervised learning methods, and unsupervised learning methods have received less attention. Unlike supervised learning methods, clustering methods do not require training. In most cases, the number of samples is limited, and deep learning methods cannot be training well, so clustering methods have a great advantage. An advantage of the proposed method is that it uses intelligent behaviour in metaheuristic algorithms and fishier mantis optimiser (FMO) algorithm to detect damaged lung areas.

3.1 Fishier mantis optimiser

In this paper, a clustering model based on the fishier mantis optimiser (FMO) algorithm is used to segment the images of COVID-19 patients. First, the FMO algorithm is formulated based on the hunting behaviour of this insect, and in the second part, this behaviour is used to cluster the COVID-19 images.

3.1.1 Behaviour of fishier mantis

Mantis is known as one of the predatory insects. They are green, locust-like insects with long legs, large heads, and two pairs of wings (Figure 1(a)). Mantis lives in the tropics, and some live in temperate regions. When the mantis stands quietly, he holds his front legs forward like two hands, and in this position, it is like reciting a prayer. After mating, the female hunts and feeds on the opposite sex. Some types of mantis can rotate their head at an angle of 180 degrees and use it to scan the environment. Most of these insects

live in the foliage of trees and disguise themselves as small branches to deceive their prey. Mantis are arthropod hunters. Most mantis are ambush hunters who feed only on the live prey available to them. They disguise themselves and stay still and wait for the victim to approach. They can chase their victim with slow movements. Sometimes mantis eats smaller ones. They also eat small vertebrates such as lizards, frogs, fish, and birds. A type of mantis is famous for its strange behaviour in hunting fish. These fish-eating insects have been hiding in a pond continuously for five days, waiting to catch a fish at the right time. The mantis can hunt two ebony fish every day. They can catch up to nine fish in five days and eat their prey over time. Figure 1(b), shows a fish-eating mantis camouflaging and hunting fish:

Figure 1 (a) Mantis and (b) fish-eating mantis (see online version for colours)

(a) (b)

The fishier mantis has a set of intelligence hunting behaviours. These insects can consider several situations and move in these situations. The optimal position for the mantis is the location of the prey or fish. The fishier mantis also has homogenous behaviours. The fishier mantis has behaviours in preparation for attacking or giving up hunting in its current state, which is described below.

3.1.2 Creating an initial population of situations

In the FMO algorithm, a fishier mantis first considers several random situations in the problem space. Each of these situations is assumed to be a solution, and the fishier mantis tries to put you in a position that is closer to the optimal solution. The initial positions or solutions in equation (1) are formulated and using the objective function, each of the situations can be evaluated according to equation (2):

$$Mantis = \begin{bmatrix} X_{11}, X_{12}, X_{13}, \ldots, X_{1d} \\ X_{21}, X_{22}, X_{23}, \ldots, X_{2d} \\ X_{31}, X_{32}, X_{33}, \ldots, X_{3d} \\ \vdots \\ X_{n1}, X_{n2}, X_{n3}, \ldots, X_{nd} \end{bmatrix} \tag{1}$$

In this equation, X_{ij} is the solution of its *i*th solution and then its *j*th. In the first iteration, a random population is created from solutions such as equation (2) [14]:

$$F(Mantis)=\begin{bmatrix} Fittness(X_{11},X_{12},X_{13},\ldots,X_{1d}) \\ Fittness(X_{21},X_{22},X_{23},\ldots,X_{2d}) \\ Fittness(X_{31},X_{32},X_{33},\ldots,X_{3d}) \\ \vdots \\ Fittness(X_{n1},X_{n2},X_{n3},\ldots,X_{nd}) \end{bmatrix} \tag{2}$$

In the equations, *Mantis* and $F(Mantis)$ are the matrices of solutions or situations and their degree of competence, respectively. In the equation in question, X_i is equal to the last *i*, and this solution has d dimensions such as $X_{i1},X_{i2},X_{i3},\ldots,X_{id}$. Equation (3) is used to create random solutions:

$$X_i = L+(U-L)\times rand(0,1) \tag{3}$$

In this equation, rand(0,1) is a random vector between zero and one with a uniform distribution. *L* and *U* are the lower and upper ranges of the problem space, respectively.

3.1.3 Reminders of situations

In the FMO algorithm, moths choose a new position to hunt, place themselves in that position, and camouflage themselves. Mantis can memorise several different states, and these optimal states in a matrix are defined as *m*. The state is $m < n$ and is defined according to equation (4):

$$States=\begin{bmatrix} S_{11},S_{12},S_{13},\ldots,S_{1d} \\ S_{21},S_{22},S_{23},\ldots,S_{2d} \\ S_{31},S_{32},S_{33},\ldots,S_{3d} \\ \vdots \\ S_{m1},S_{m2},S_{m3},\ldots,S_{md} \end{bmatrix} \tag{4}$$

The status matrix holds states. It is assumed that the value of optimality is proportional to the maximum of solutions. It is assumed that the mantis keeps these limited conditions in its memory and hunts mainly in these areas.

3.1.4 Moving towards optimal situations

Each time the status matrix is updated, the mantis has better conditions to locate in the matrix. A mantis can randomly select an optimal situation and move towards it, as in equation (5), and take a position in it:

$$X_i^{new} = X_i + Walk.(States(j)-X_i)\times rand(0,1) \tag{5}$$

X_i is the current position of a mantis, X_i^{new} is the new position of a mantis, $States(j)$ is a random state and *j* is a random member calculated from Equation (6):

$$j = 1+\left[rand\times(m-1)\right] \tag{6}$$

The walk is the size of the mantis's step towards the desired solution. The value of the walk parameter is reduced by the iteration of the FMO algorithm because it is assumed

that the mantis reduces step size. In contrast, the mantis closes the prey or the optimal solution. To change the walk parameter of relation (7), it is suggested:

$$Walk = \left[1 - \frac{it}{MaxIt}\right] \tag{7}$$

In this respect, it is the current iteration number. The value of the MaxIt is the final iteration number of the algorithm. To apply a more random behaviour, the Chebyshev random function is used, and the criterion of the desired function is according to equation (8). The step relation is formulated as equation (9):

$$u_{i+1} = \cos\left(icos^{-1}\left(u_i\right)\right), u_1 = 0.7 \tag{8}$$

$$Walk = \left[1 - \frac{it}{MaxIt}\right].u_{i+1}, u_{i+1} = \cos\left(icos^{-1}\left(u_i\right)\right), u_1 = 0.7 \tag{9}$$

In the diagram of Figure 2(a), a random sequence is shown, and in Figure 2(b), the random step function is plotting to move the mantis insect in the problem space. The maximum number of iterations of the proposed algorithm is 100. The step reduction changes the nature of the search from global to local search in terms of the algorithm iteration.

Figure 2 (a) Random sequence and (b) steps of a fishier mantis based on a random sequence (see online version for colours)

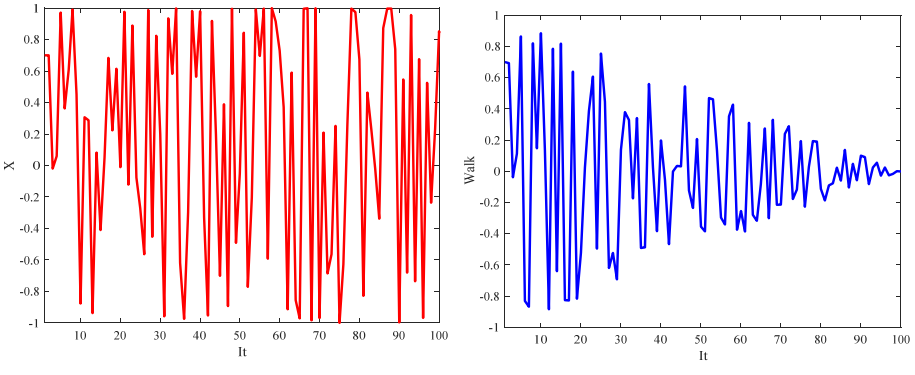

(a) (b)

3.1.5 Override moving towards optimal positions

Any solution or mantis can ignore the previous optimal situations and look for a random position. Random position selection improves the algorithm's global search and reduces the likelihood of convergence to local optimisations. To model this behaviour, equation (10) be used:

$$X_i^{new} = \begin{cases} L + (U - L) \times rand(0,1) & r < 0.5 \\ \frac{L+U}{2} + (X^* - \frac{L+U}{2}) \times rand(0,1) & 0.5 \le r \end{cases} \tag{10}$$

The value of *r* is a random number between zero and one.

3.1.6 Using all optimal situations

Each solution or mantis can consider the previous optimal conditions and use the knowledge of all of them. It also searches for the space between the mean and the optimal state it has achieved so far, as in Equation (11):

$$X_i^{new} = \begin{cases} Walk.X_i + (\overline{States} - X^*) \times rand(0,1) & rand < 0.5 \\ Walk.X_i + (X^* - \overline{States}) \times rand(0,1) & rand \geq 0.5 \end{cases} \tag{11}$$

In this equation, $\overline{States}$ is the average number of optimal solutions and is calculated like equation (12):

$$\overline{States} = \frac{\sum_{i=1}^{m} State_i}{m} \tag{12}$$

In the proposed method, by increasing the iteration counter and approaching the mantis to the prey, the number of situations is reduced based on the iteration of the algorithm, such as equation (13). The value of *m* is the number of initial states and $m(t)$ is the number of states in iteration *t*:

$$m(t) = m - \frac{m.it}{MaxIt} \tag{13}$$

3.1.7 Flowchart of fishier mantis optimiser (FMO) algorithm

The flowchart of the proposed method or FMO algorithm is shown in Figure 3. According to the flowchart of the proposed method, the following steps are performed in the FMO algorithm to find the optimal solution:

- Algorithm parameters such as population number, number of iterations, and objective function are setting.
- Several solutions are produced in the problem space as the position of the mantis is random.
- Each solution or position is evaluating with the Cost-function then several optimal solutions are stored in each iteration.
- Each member of the mantis population can update their position based on optimal positions or randomly select a situation in the problem space to move.
- A solution can search with equal probability for the space between the most optimal situation and one of the optimal solutions.
- The optimal position is updating in each iteration, and the size of the movement step and the sign of position storage modes also change.
- In the last iteration, the optimal position is the optimal problem.

Figure 3 Flowchart of fishier mantis optimiser (FMO) algorithm

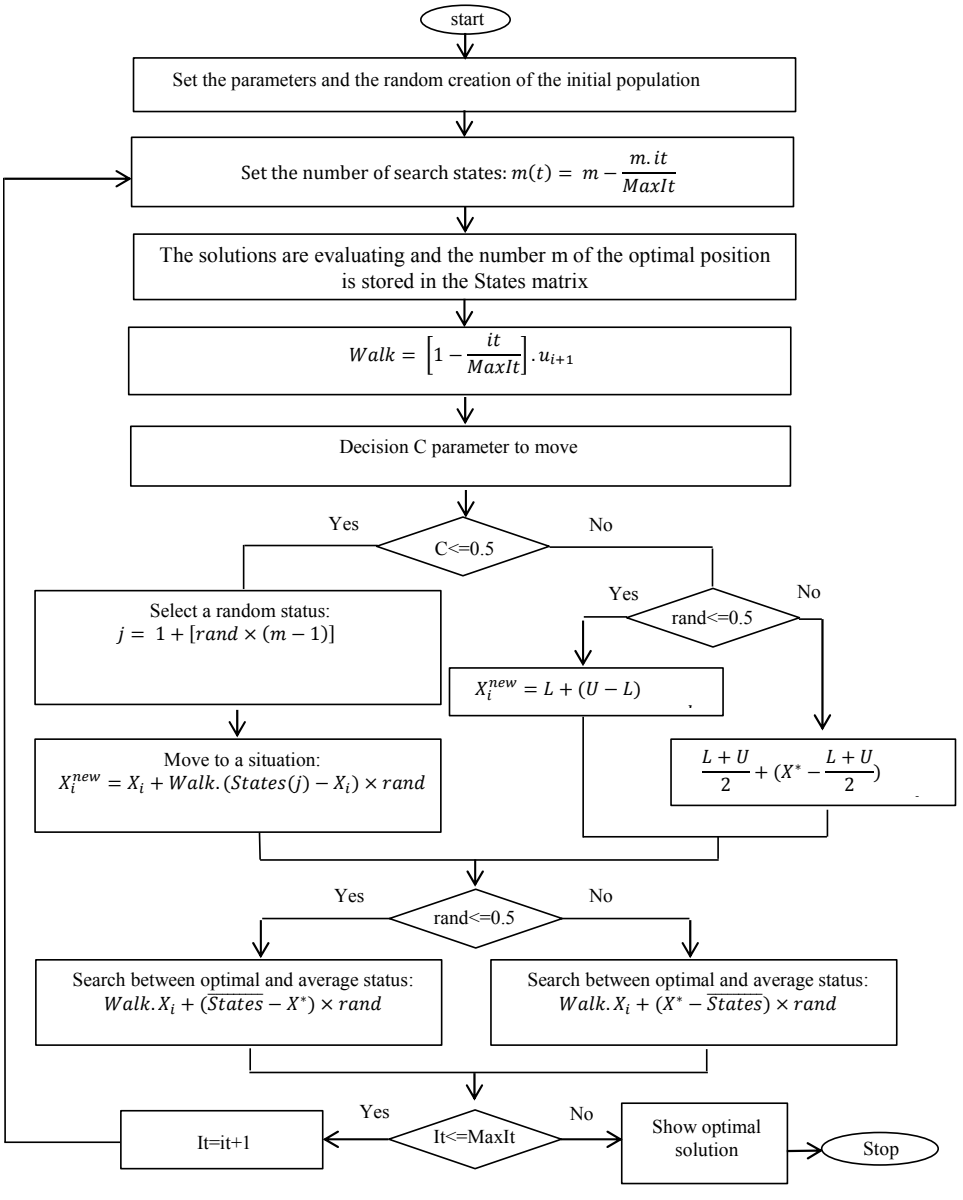

3.2 Proposed clustering

Clustering is one of the most important data mining techniques in discovering hidden patterns. In this data mining technique, each data be clustering according to its similarity to other data. In clustering methods, unlike classification methods, data labels are not used to separate the data, and clustering is performed based on the similarity of the data with the centers of the clusters. Data clustering applies to one or more properties of data and samples, such as the brightness of images.

3.2.1 Clustering objective function

To cluster the images associated with COVID-19, there are several pixels of p, each with a light intensity between zero and 255. The image pixels are according to equation (14) in a set:

$$I = \{X_1, X_2, X_3, \ldots, X_p\} \tag{14}$$

In this regard, I image is related to CT scan of patients or healthy individuals of COVID-19. Value of X_i is also the optical information of the ith pixel. The purpose of clustering is to place the specimens within k of the cluster (equation (15)) so that the objective function of equation (16) is minimised:

$$Z = \{C_1, C_2, C_3, \ldots, C_k\} \tag{15}$$

$$Cost = \sqrt{\sum_{i=1}^{p}\sum_{j=1}^{k} w_{ij} X_i - C_j^{\,2}} \tag{16}$$

In the objective function, the weight value w_{ij} is assessing according to the condition of equation (17):

$$w_{ij} = \begin{cases} 1 & X_i - C_j = min_{1 \le j \le p} X_i - C_j \\ 0 & \text{otherwise} \end{cases} \tag{17}$$

In the proposed method, the fish-eating mantis optimisation algorithm is using to minimise the clustering objective function. Each mantis is considered as a vector such as equation (18), which is a set of cluster centers. A number of these random cluster centers are created as populations of FMO algorithms and attempts are made to optimise them by this algorithm.

3.2.2 Binarising segmentation images

CT scan images are considered as input in the proposed method then a grey image is created after segmentation. The proposed method uses Otsu thresholding to accurately detect damaged tissue to reduce the number of light intensity levels to zero and one. By applying Otsu thresholding to the proposed segmentation and clustering output, the affected areas and tissues of COVID-19 can be well separated. In Otsu thresholding, the sum of the weights or frequencies of the two classes to the left and right of threshold t can be calculated as equations (18) and (19), respectively, and the sum of these two weights to the right and left of the classes is also equal to one [28]:

$$w_0 = \sum_{i=0}^{t-1} p_i \tag{18}$$

$$w_1 = \sum_{i=t}^{L-1} p_i \tag{19}$$

In the next phase, the weighted average of the left and right sides of the threshold is calculated according to equations (20) and (21). Using this mechanism, according to equation (22), the average of the two classes, left and right, is the threshold. In the next

step, using the weights of the two classes and the calculated mean, such as equation (24), the appropriate objective function is formulated. In this case, the goal is to maximise the objective function by finding the optimal thresholds [28]:

$$\mu_0 = \sum_{i=0}^{t-1} \frac{i.p_i}{\omega_0} \tag{20}$$

$$\mu_1 = \sum_{i=t}^{L-1} \frac{i.p_i}{\omega_1} \tag{21}$$

$$\mu_T = \omega_0.\mu_0 + \omega_1.\mu_1 \tag{22}$$

$$f = \omega_0.(\mu_0 - \mu_T)^2 + \omega_1.(\mu_1 - \mu_T)^2 \tag{23}$$

In this regard, μ_0 and μ_1 are the weighted average light intensity of the two classes of left and right threshold pixels, respectively. The μ_T is the weighted mean light intensity of the two sides of the thresholding.

4 Experiments and analysis

The analysis and evaluation of the proposed method are done in two stages. First, using the evaluation functions, the accuracy of the FMO algorithm is compared with similar techniques. In the second phase, this method is used for clustering and segmentation of lung CT-Scan images to diagnose COVID-19 disease.

4.1 Convergence analysis

In this section, benchmark functions are introducing. We will use some of these functions to analyse the accuracy and optimal calculation error in the FMO algorithm.

4.1.1 Benchmark functions

To measure the efficiency and accuracy of meta-heuristic algorithms, standard objective functions or costs are required to use as standard benchmark functions. Many studies related to meta-heuristic algorithms typically use cost functions as benchmark functions. Benchmark functions are a set of mathematical functions in which the essential purpose is to find the global minimum. In the proposed method are used 13 widely used CEC functions (Table 1). CEC functions are used in most studies to evaluate meta-heuristic algorithms.

4.1.2 Implementation parameters

Benchmark functions are using to analyse the FMO algorithm. In the implementations, in addition to implementing the FMO algorithm, other meta-heuristic algorithms such as particle swarm optimisation algorithm, grasshopper optimisation algorithm (GOA), spotted hyena optimiser (SHO) algorithm, Harris hawks optimisation algorithm, black widow optimisation algorithm (BWO), and atom search algorithm are implemented and

compared with the proposed method. The population size of each algorithm is 15, the number of iterations is 100, and the number of tests of each algorithm on each of the evaluation functions is 30. In the FMO algorithm, the initial value of *m* is equal to 0.5 or half of the initial population. The PSO algorithm's individual and group learning coefficients are equal to 2, and its inertia coefficient is equal to 0.8. The Cmax and Cmin coefficients of the GOA algorithm are 0.1 and 0.001, respectively. The initial value of the parameter h in the SHO algorithm is 5. In the HHO algorithm, the value of E is a random number in the range [–2, + 2]. The pp and pm coefficients in the BWO algorithm are 0.6 and 0.4, respectively. The values of Depth weight and Multiplier weight in the ASO algorithm are 50 and 0.2, respectively. The meta-heuristic algorithms are comparing in the mean index of optimal calculation error and the mean of convergence in local optimisations [29]:

Table 1 Benchmark functions to measure the accuracy of the proposed method

Function	*Dim*	*Range*	$f_{\min}$
$F1(x)=\sum_{i=1}^{n}x_i^2$	10	[−100,100]	0
$F2(x)=\sum_{i=1}^{n}\lvert x_i\rvert+\prod_{i=1}^{n}\lvert x_i\rvert$	10	[−10,10]	0
$F3(x)=\sum_{i=1}^{n}\left(\sum_{j-1}^{i}x_j\right)^2$	10	[−100,100]	0
$F4(x)=\max_i\{\lvert x_i\rvert,1\le i\le n\}$	10	[−100,100]	0
$F5(x)=\sum_{i=1}^{n-1}[100(x_{i+1}-x_i^2)^2+(x_i-1)^2]$	10	[−30,30]	0
$F6(x)=\sum_{i=1}^{n}([x_i+0.5])^2$	10	[−100,100]	0
$F7(x)=\sum_{i=1}^{n}ix_i^4+\text{random}[0,1)$	10	[−1.28,1.28]	0
$F8(x)=\sum_{i=1}^{n}-x_i\sin(\sqrt{\lvert x_i\rvert})$	10	[−500,500]	−418.9829 × 5
$F9(x)=\sum_{i=1}^{n}[x_i^2-10\cos(2\pi x_i)+10]$	10	[−5.12,5.12]	0
$F10(x)=-20\exp\left(-0.2\sqrt{\frac{1}{n}\sum_{i=1}^{n}x_i^2}\right)-\exp(\frac{1}{n}\sum_{i=1}^{n}\cos(2\pi x_i))+20+e$	10	[−32,32]	0

Table 1 Benchmark functions to measure the accuracy of the proposed method (continued)

Function	*Dim*	*Range*	$f_{\min}$
$F11(x)=\frac{1}{4000}\sum_{i=1}^{n}x_i^2-\prod_{i=1}^{n}\cos(\frac{x_i}{\sqrt{i}})+1$	10	[−600,600]	0
$\mathrm{F12}(x)=\frac{\pi}{n}\left\{10\sin(\pi y_1)+\sum_{i=1}^{n-1}(y_i-1)^2\left[1+10\sin^2(\pi y_{i+1})\right]+(y_n-1)^2\right\}+\sum_{i=1}^{n}u(x_i,10,100,4)\,y_i=1+\frac{x_i+1}{4}$	10	[−50,50]	0
$u(x_i,a,k,m)=\begin{cases}k(x_i-a)^m & x_i>a\\ 0 & -a<x_i<a\\ k(-x_i-a)^m & x_i<-a\end{cases}$			
$\mathrm{F13}(x)=0.1\{\sin^2(3\pi x_1)+\sum_{i=1}^{n}(x_i-1)^2[1+\sin^2(3\pi x_i+1)]+(x_n-1)^2[1+\sin^2(2\pi x_n)]\}+\sum_{i=1}^{n}u(x_i,5,100,4)$	10	[−50,50]	0

4.1.3 Convergence analysis in terms of iteration

A suitable method for evaluating the FMO algorithm is to measure the optimal calculation error in terms of iteration and compare it with similar algorithms such as PSO, GOA, ASO, HHO, and BWO algorithms. In the diagram of Figure 4, the four output samples of the proposed method and its comparison with other meta-heuristic algorithms are comparing. In these experiments, the average global computational error of the algorithm is comparing in terms of iteration:

The implementation results on most benchmark functions show that the proposed method for finding the optimal global evaluation or objective functions is more accurate than the PSO, GOA, ASO, HHO, and BWO algorithms. The error of the optimal calculation of benchmark functions in the last iteration in the FMO algorithm is less than other methods. Diagram analysis shows that the slope of reducing the optimal calculation error in terms of repetition of the FMO algorithm is higher than another algorithm. Experiments show that the optimal calculation error is reduced faster in terms of iteration. Diagram analysis shows that the solution population in the FMO algorithm is directing to the optimal solutions with more intelligence and speed.

4.1.4 Analysis of error-index and standard deviation

The rank of the algorithms is calculating by finding the optimal answer with the Wilcoxon test. Any algorithm that can show a lower number and a near one has less error. In most experiments, it is ranked first in terms of optimal accuracy. Figure 5 shows the average rank of the proposed algorithm and other algorithms in the optimal

calculation error index. The standard deviation of the optimal calculation error is a suitable criterion for measuring the stability of algorithms, which is shown in Figure 6.

Figure 4 Error measurement and comparison on benchmark functions F1, F5, F9 and F10 (see online version for colours)

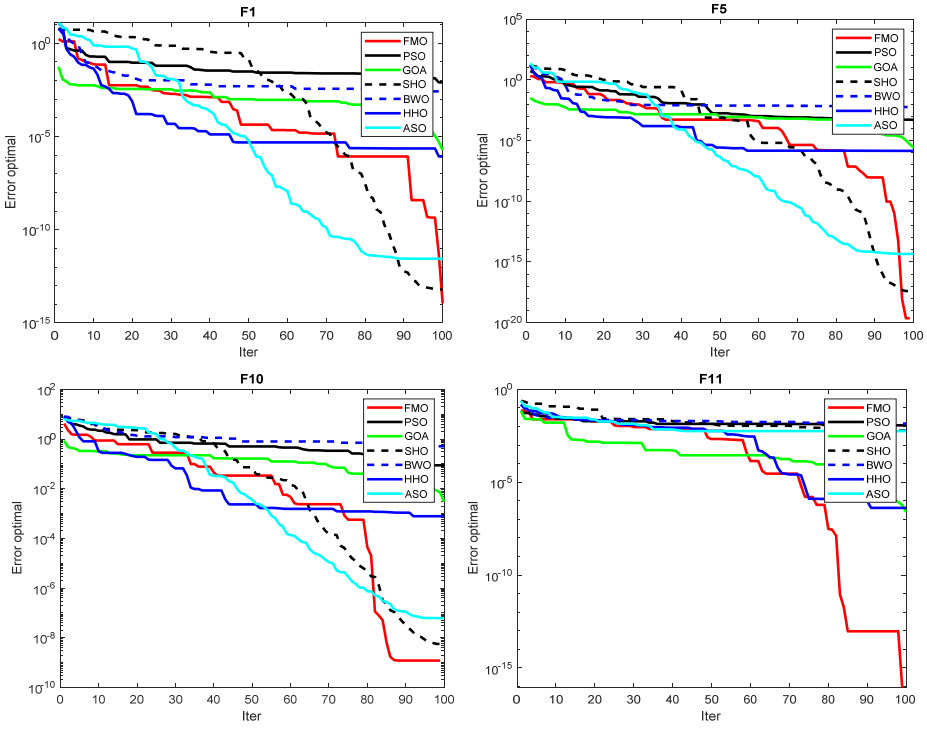

Figure 5 Rank of the proposed algorithm and other algorithms in the mean error-index (see online version for colours)

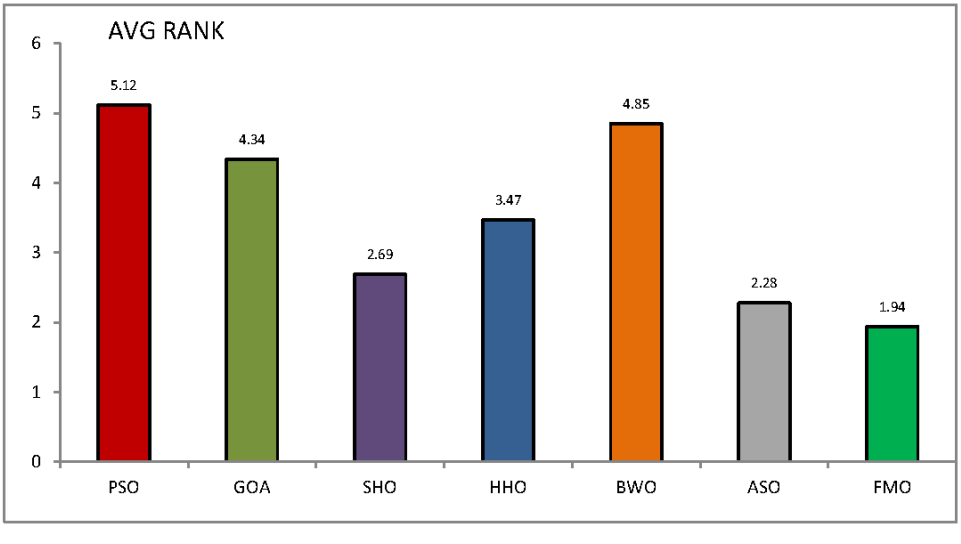

Figure 6 Rank of the proposed algorithm and other algorithms in the mean standard deviation index (see online version for colours)

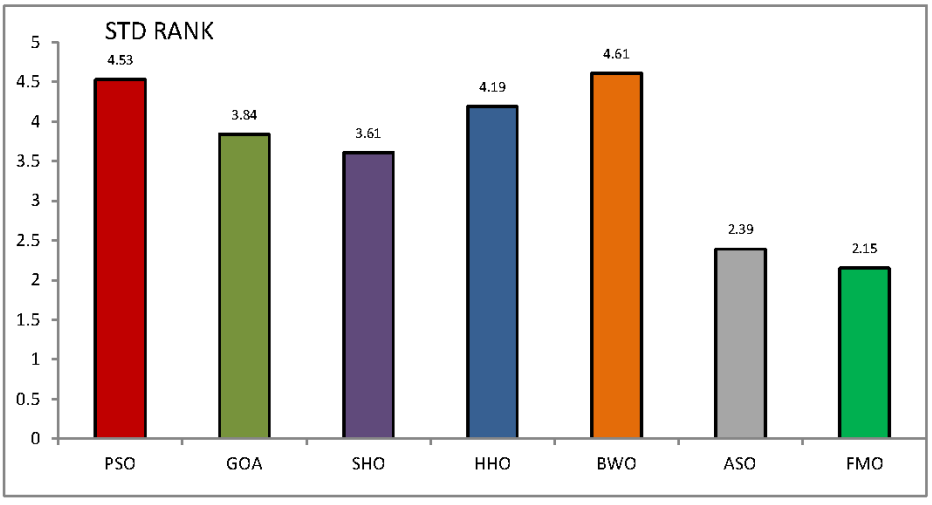

The analysis of the proposed algorithm with the global average optimal error index shows that the error rating of the FMO algorithm is 1.94 and is the lowest error among the methods compared. In most experiments, the proposed method ranks first with the least error. ASO and SHO algorithms have the next ranks in terms of error minimisation.

Experiments showed that the PSO algorithm had the highest error and the worst performance among the methods compared. Optimal computational standard deviation is also an important indicator in evaluating algorithms and measuring their stability. If an algorithm can achieve fewer errors for optimal calculation with less standard deviation, it indicates that the algorithm is more stable to find the optimal solution. Among the algorithms, the best rank in terms of standard deviation is related to the FMO algorithm, which has a ranking of 2.15. The atom search algorithm ranks second in terms of standard deviation. The worst of them are related to the BWO algorithm and the PSO algorithm. The high stability of the FMO algorithm indicates that the algorithm has more certainty in finding the optimal solution.

4.2 Segmentation analysis

In this section, the FMO algorithm is using to segment the COVID-19 images. First, the dataset is introduced, and then the accuracy of the proposed method in clustering and minimising the objective function of clustering is compared with other methods. In the following, the proposed method is comparing with several scanning image segmentation methods.

4.2.1 Image collection

The first phase is from a numerical dataset in a Brazilian hospital and includes 19 patients in the early months of 2020. It is using to measure clustering efficiency in the FMO algorithm. This dataset has 600 instances. The 19 features use to diagnose COVID-19. Feature No. 20 is the output type, which indicates the type of label of the person in

healthy or infected with infection. The second dataset is related to the segmentation of COVID-19 images and is available from Kaggle.

4.2.2 Evaluation of the clustering objective function

In clustering, the number of clusters was considered equal to 2, one cluster representing healthy people and one cluster representing Infected people. The population size of the meta-heuristic algorithms and the proposed method is 15, and the number of iterations is 30, and each experiment is repeated 25 times. The similarity index is Euclidean, cosine, and Manhattan, which are shown in relations (24)–(26), respectively [30]:

$$d_E(x,y) = \sqrt{\sum_{i=1}^{n}(x_i - y_i)^2} \tag{24}$$

$$cos(x,y) = \frac{\sum_{i=1}^{n} x_i . y_i}{\left[\sum_{i=1}^{n} x_i^2 \sum_{i=1}^{n} y_i^2\right]^{1/2}} \tag{25}$$

$$M(x,y) = \sum_{i=1}^{n} |x_i - y_i| \backslash \tag{26}$$

$d_E(x,y)$, cos (x, y) and M (x, y) are the criteria for Euclidean, cosine, and Manhattan similarity, respectively. x_i and y_i are the feature vectors of two data belonging to the dataset. The results of the clustering method implementation by the proposed method and its comparison with the PSO, GOA, SHO, and HHO algorithm in three similarity indices are shown in Figures 7–9.

Figure 7 Comparison of reduction of the objective function with Euclidean similarity index (see online version for colours)

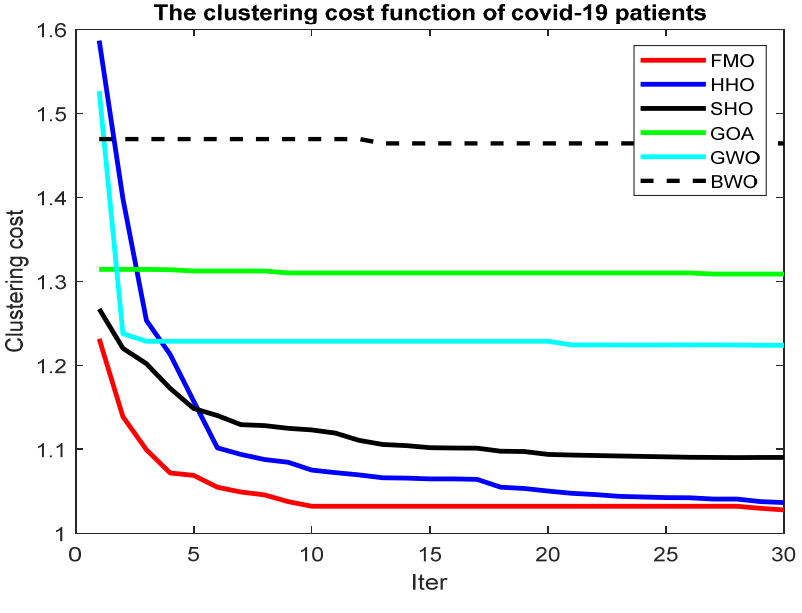

Figure 8 Comparison of reduction of the objective function with cosine similarity index (see online version for colours)

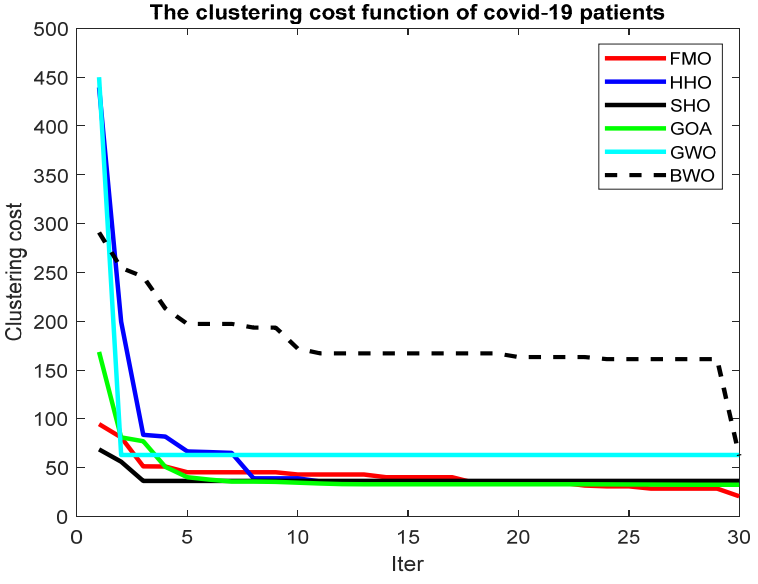

Figure 9 Comparison of reduction of the objective function with Manhattan similarity index (see online version for colours)

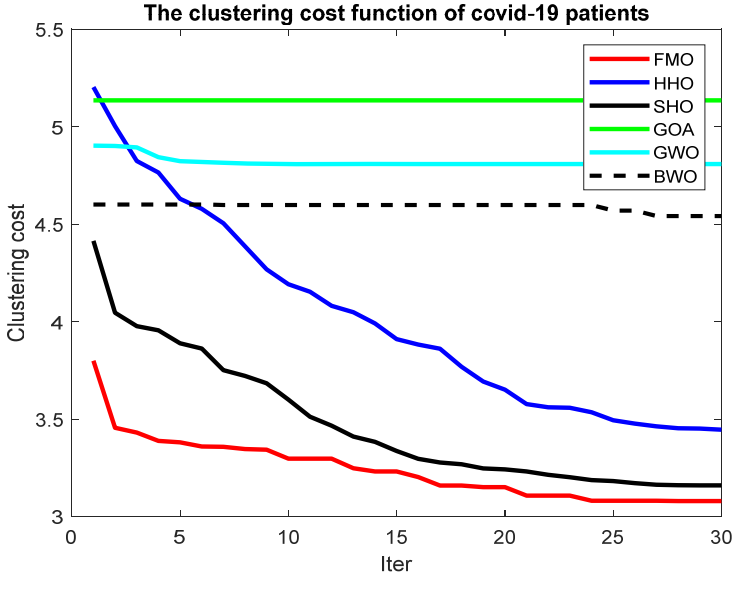

The analysis shows that the proposed method reduces the clustering objective function further than other algorithms. Reducing the objective function in the proposed method is more than other methods in terms of the iteration of meta-heuristic algorithms. In the last iteration, the proposed algorithm ultimately reduces the clustering objective function compared to similar methods. This reduction is further due to the optimal selection of

clustering centers. In the diagrams of Figures 10–12, the average clustering objective function of the proposed method is comparing with three Euclidean, cosine, and Manhattan similarity indices with similar methods:

Figure 10 Comparison of the objective function with the Euclidean similarity index (see online version for colours)

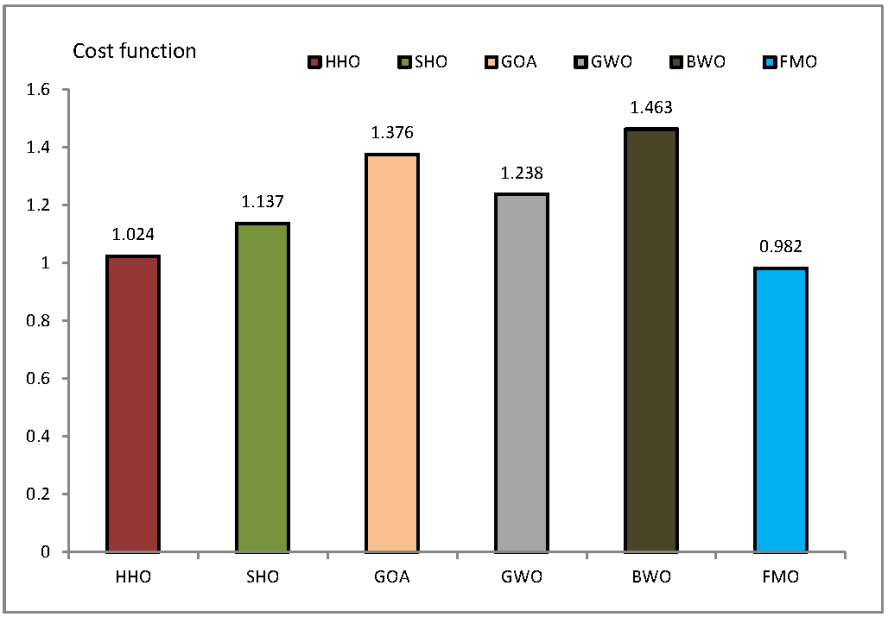

Figure 11 Comparison of the objective function with the cosine similarity index (see online version for colours)

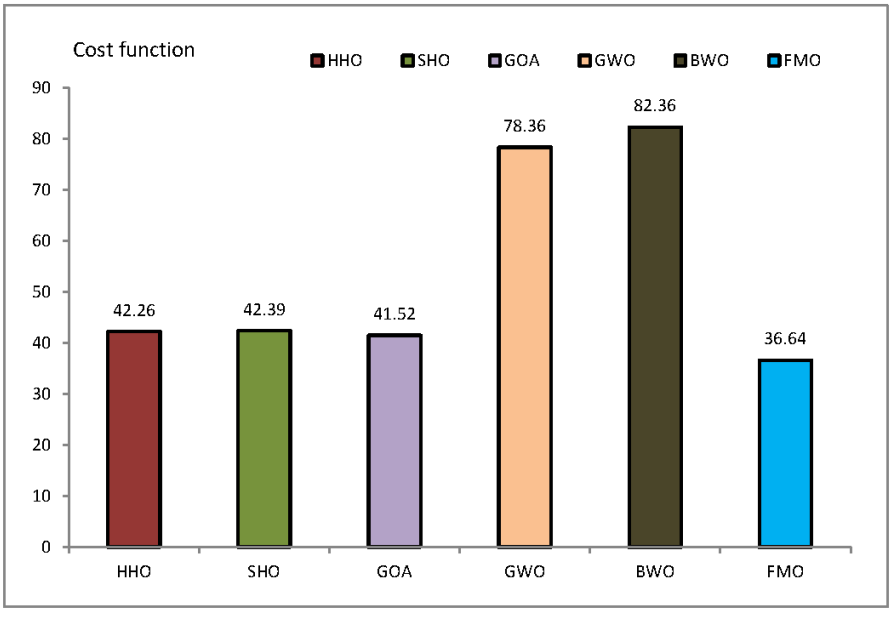

Figure 12 Comparison of the objective function with Manhattan similarity index (see online version for colours)

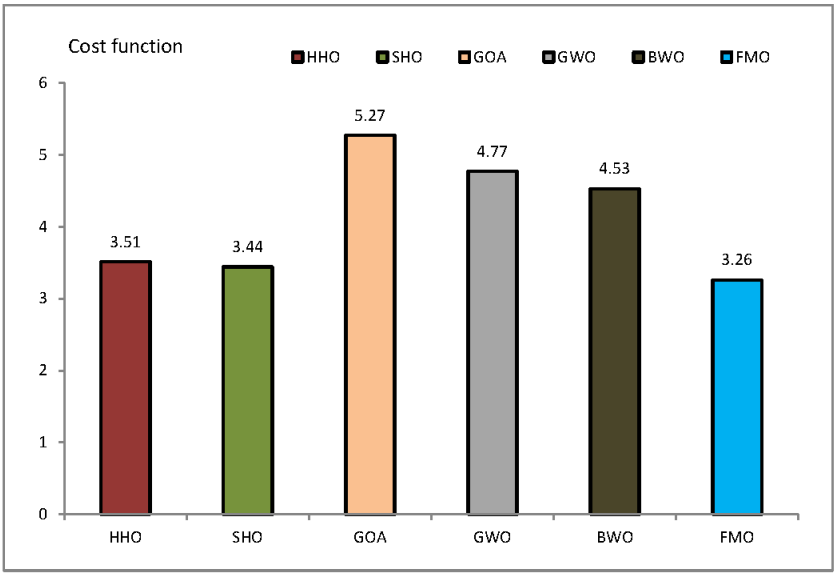

Analysis and evaluation of clustering objective function diagrams show the value of clustering objective function with Euclidean similarity index in HHO algorithm, SHO algorithm, GOA algorithm, GWO algorithm, BWO algorithm, and proposed algorithm of 1.024, 1.13, respectively. 1.376, 1.238, 1.463 and 0.982. The proposed method in reducing the objective function of clustering with the Euclidean index has the first ranking, then the HHO algorithm is in the second place, and the worst method is related to the BWO algorithm.

The objective function with cosine index in HHO algorithm, SHO algorithm, GOA algorithm, GWO algorithm, BWO algorithm, and the proposed algorithm is 42.26, 42.39, 41.52, 78.36, 82.36, and 36.64, respectively. The proposed method further reduces the objective function in the cosine index than other methods. The objective function in the Manhattan index and the clustering methods is 3.51, 3.44, 5.27, 4.77, 4.53, and 3.26, respectively. The proposed method in this index also reduces the clustering objective function more than other methods and is in the next rank of the SHO and HHO algorithm.

4.2.3 Segmentation of CT scan images

In this section, the proposed algorithm for clustering and zoning CT images of lung scan to diagnose COVID-19 disease. The problem in this section is a classification issue that aims to classify images into two categories: COVID-19 and healthy.

4.2.3.1 CT-Scan images

Grey images related to CT scans of the lungs use for segmentation, clustering, and distributing images to healthy and COVID-19 individuals. In the implementations, 876 CT scan images of the lungs are using. There are 438 images of healthy people and

438 images related to damaged lungs in this dataset. In Figure 13, some of these images can be seen[1] [31]:

Figure 13 Top-row images associated with COVID-19 patients and bottom-row images associated with healthy individuals

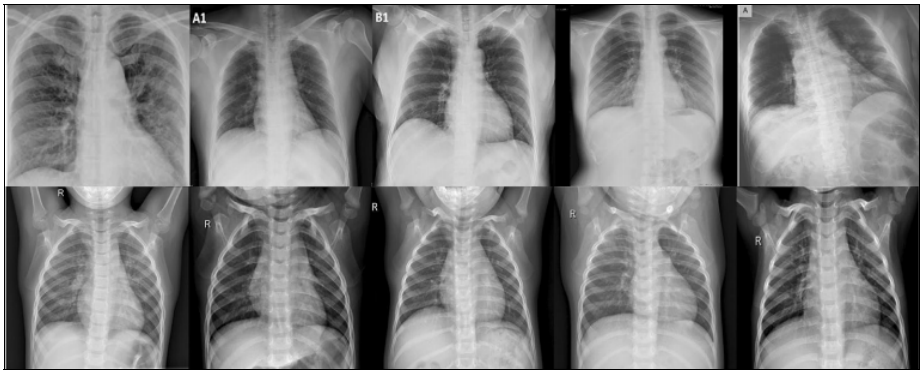

4.2.3.2 Evaluation criteria

In this study, three criteria of accuracy, sensitivity, and similarity index according to relations (27)–(29) are used to evaluate and classify images into two categories of COVID-19 and healthy [32–38]:

$$Accuracy = \frac{TP + TN}{TP + TN + FP + FN} \tag{27}$$

$$Sensitivity = \frac{TP}{TP + FN} \tag{28}$$

$$SI = \frac{2 \times TP}{2 \times TP + FP + FN} \tag{29}$$

Compare real and segmentation images to measure TP, TN, FP, and FN indices. In the evaluations, the value of *P* means positive for the disease and *N* means healthy, and *T* and *F* indicate the correct or incorrect classification of the image, respectively.

4.2.3.3 Evaluating the diagnosis of patients with COVID-19

In addition to the proposed method for diagnosing COVID-19 disease, the HHO algorithm, SHO algorithm, GOA algorithm, GWO algorithm, BWO algorithm have been used in the evaluations, and the proposed method compares with these methods. The Euclidean similarity index considers in the measurements. The mean accuracy, sensitivity, and similarity index for the diagnosis of COVID-19 disease are compared in Table 2 and the diagrams in Figures 14–16.

Table 2 Comparison of the proposed method in detecting COVID-19

Methods	*SI*	*Accuracy*	*Sensitivity*
HHO	98.12	98.03	97.88
SHO	98.03	97.84	97.54
GOA	97.73	97.69	97.64
GWO	97.87	97.66	97.52
BWO	97.32	97.11	97.08
FMO	98.63	98.45	98.37

Figure 14 Comparison of the proposed method with other methods in the similarity index (see online version for colours)

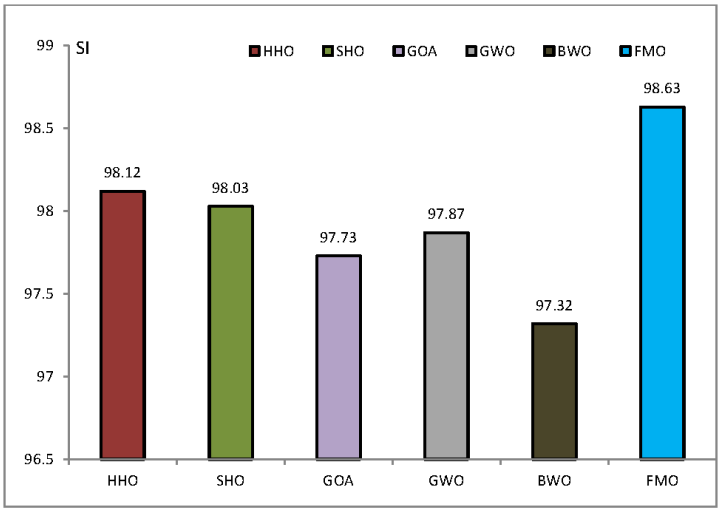

Figure 15 Comparison of the proposed method with other methods in the accuracy index (see online version for colours)

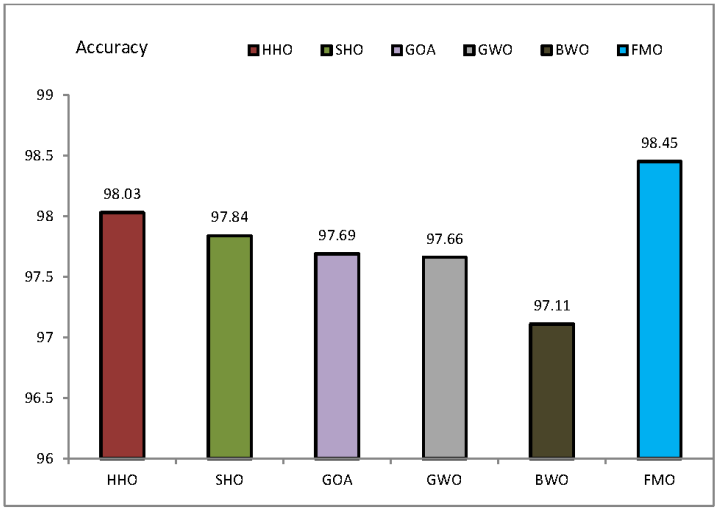

Figure 16 Comparison of the proposed method with other methods in the sensitivity index (see online version for colours)

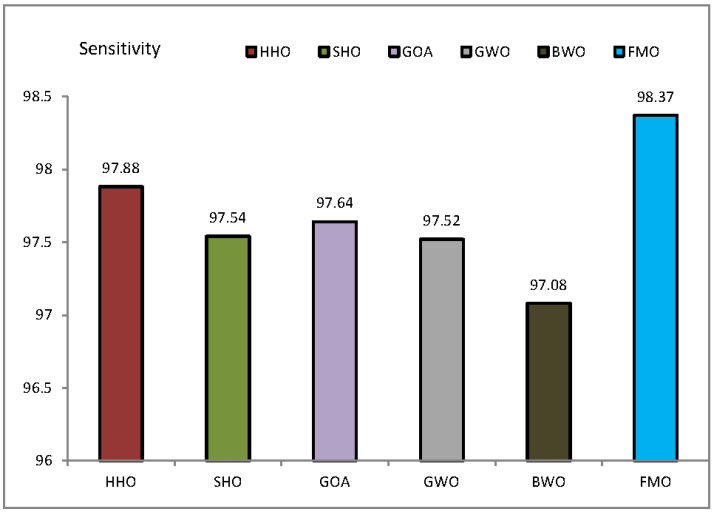

Analysis and evaluations show that the similarity index for distinguishing COVID-19 patients from healthy individuals in the HHO algorithm, SHO algorithm, GOA algorithm, GWO algorithm, BWO algorithm, and the proposed method is 98.12%, 98.03%, 97.73%, 97.87%, 97.32%, and 98.63% respectively. The proposed method has the highest similarity index in the diagnosis of COVID-19 patients. The accuracy of diagnosis of COVID-19 patients in the methods is 98.03%, 97.84%, 97.69%, 97.66%, 97.11% and 98.45%, respectively. The sensitivity index in these methods is 97.88%, 97.54%, 97.64%, 97.08% and 98.37%, respectively.

Experiments show that the proposed method in diagnosing the disease is more accurate in the similarity, accuracy, and sensitivity index than the HHO algorithm, the SHO algorithm, the GOA algorithm, the GWO algorithm, and the BWO algorithm.

For computational complexity, we can say that the most common sources are time (amount of time required to solve the problem) and space (amount of memory needed). Other sources include the number of parallel processors (in parallel processing mode). But the above factors are not discussed here. It should be noted that the theory of complexity is different from the theory of solvability. This theory argues that a problem can be solved regardless of the resources required. There are cases when we know that a problem has an answer, but the solution and method of solving it have not been provided yet. Sometimes, in addition to the mentioned problem, even with the solution in hand, we do not have the necessary resources and tools to implement that problem.

5 Conclusion

COVID-19 disease has become a challenge in the world. Millions of people are infecting with the disease. Estimates show that millions of people will die from the disease. One way to deal with this disease is to use diagnosing and CT-Scan patients from healthy people to break the chain of the disease. One of the most important ways to diagnose

COVID-19 disease is to use CT scans of the lungs, which diagnostician infected people from healthy people. Due to many patients and the referral of healthy and infected people to medical centers in a way that can automatically diagnose the disease in people is essential and vital. In this paper, for diagnosing COVID-19 disease, the segmentation method based on clustering of lung CT scan images and data collected from medical centers has been used. First, a meta-heuristic algorithm is introduced based on the intelligence behaviour of fishier mantis, and then a copy of it is presented for clustering and segmentation. Experiments show that the FMO algorithm is more accurate in finding the optimal solution in the benchmark functions than the PSO, GOA, SHO, HHO, BWO, and ASO algorithms. The dataset of COVID-19 patients in one of the Brazilian hospitals was used to analyse the proposed method. The analyses showed that the proposed method was more accurate than the PSO, GOA, SHO, HHO, BWO, and ASO algorithms in clustering COVID-19 images. Analyses show that the proposed method in classifying images of infected and healthy people has a similarity, accuracy, and sensitivity index of 98.63%, 98.45%, and 98.37%, respectively. The proposed method is more accurate than the HHO algorithm, the SHO algorithm, the GOA algorithm, the GWO algorithm, and the BWO algorithm. In a future study, the FMO algorithm selects features in the diagnosis of COVID-19 patients from CT scan images. We recommend applying artificial intelligence methods like the deep learning method and finding the true values for optimisation parameters used in the FMO method for future scope.

References

1 Lima-Costa, M.F., Macinko, J., de Andrade, F.B., de Souza Júnior, P.R.B., de Vasconcellos, M.T.L. and de Oliveira, C.M. (2020) 'ELSI COVID-19 initiative: methodology of the telephone survey on coronavirus in the Brazilian longitudinal study of aging', *Cad. Saude Publica*, Vol. 36, p.e00183120.

2 Beck, B.R., Shin, B., Choi, Y., Park, S. and Kang, K. (2020) 'Predicting commercially available antiviral drugs that may act on the novel coronavirus (SARS-CoV-2) through a drug-target interaction deep learning model', *Comput. Struct. Biotechnol J.*, Vol. 18, March, pp.784–790, doi: 10.1016/j.csbj.2020.03.025. PMID: 32280433; PMCID: PMC7118541.

3 Huang, J.Z., Han, M.F., Luo, T.D., Ren, A.K. and Zhou, X.P. (2020) 'Mental health survey of 230 medical staff in a tertiary infectious disease hospital for COVID-19', *Zhonghua Lao Dong Wei Sheng Zhi Ye Bing Za Zhi=Zhonghua Laodong Weisheng Zhiyebing Zazhi=Chinese J, Ind. Hyg. Occup. Dis.*, Vol. 38, pp.E001–E001.

4 Vidal, P.L., de Moura, J., Novo, J. and Ortega, M. (2020) *Multi-Stage Transfer Learning for Lung Segmentation using Portable X-ray Devices for Patients with COVID-19*, ArXiv Prepr. ArXiv2011.00133.

5 Oulefki, A., Agaian, S., Trongtirakul, T. and Laouar, A.K. (2020) 'Automatic COVID-19 lung infected region segmentation and measurement using CT-scans images', *Pattern Recognit.*, p.107747.

6 Ippolito, D., Ragusi, M., Gandola, D., Maino, C., Pecorelli, A., Terrani, S., Peroni, M., Giandola, T., Porta, M., Talei Franzesi, C. and Sironi, S. (2020) 'Computed tomography semi-automated lung volume quantification in SARS-CoV-2-related pneumonia', *Eur. J. Radiol.*, pp.1–11.

7 Wu, W., Gao, L., Duan, H., Huang, G., Ye, X. and Nie, S. (2020) 'Segmentation of pulmonary nodules in CT images based on 3D-UNET combined with three-dimensional conditional random field optimization', *Med. Phys.*, Vol. 47, No. 9, pp.4054–4063.

8 Javor, D., Kaplan, H., Kaplan, A., Puchner, S.B., Krestan, C. and Baltzer, P. (2020) 'Deep learning analysis provides accurate COVID-19 diagnosis on chest computed tomography', *Eur. J. Radiol.*, Vol. 133, p.109402.

9 Zhang, T. and Lin, G. (2020) *Generalized k-means in GLMs with Applications to the Outbreak of COVID-19 in the United States*, ArXiv Prepr. ArXiv2008.03838.

10 Ahsan, M.M., Alam, T.E., Trafalis, T. and Huebner, P. (2020) 'Deep MLP-cNN model using mixed-data to distinguish between COVID-19 and non-COVID-19 patients', *Symmetry* (*Basel*)., Vol. 12, No. 9, p.1526.

11 Shahid, F., Zameer, A. and Muneeb, M. (2020) 'Predictions for COVID-19 with deep learning models of LSTM, GRU and bi-LSTM', *Chaos, Solitons Fractals*, Vol. 140, p.110212.

12 Özkaya, U., Öztürk, Ş., Budak, S., Melgani, F. and Polat, K. (2020) *Classification of COVID-19 in Chest CT Images Using Convolutional Support Vector Machines*, ArXiv Prepr. ArXiv2011.05746.

13 Chen, T. and Lin, C-W. (2020) 'Smart and automation technologies for ensuring the long-term operation of a factory amid the COVID-19 pandemic: an evolving fuzzy assessment approach', *Int. J. Adv. Manuf. Technol*., pp.1–14.

14 Patibandla, R.S.M.L. and Narayana, V.L. (2021) 'Computational intelligence approach for prediction of COVID-19 using particle swarm optimization', *Computational Intelligence Methods in COVID-19: Surveillance, Prevention, Prediction and Diagnosis*, Springer, pp.175–189.

15 Sahu, S.P., Kumar, R., Londhe, N.D. and Verma, S. (2021) 'Segmentation of lungs in thoracic CTs using K-means clustering and morphological operations', *Advances in Biomedical Engineering and Technology*, Springer, pp.331–343.

16 Raj, S., Vinod, D.S., Mahanand B.S. and Murthy, N. (2020) 'Intuitionistic fuzzy C means clustering for lung segmentation in diffuse lung diseases', *Sens. Imaging*, Vol. 21, No. 1, pp.1–16.

17 Kishor, A. and Chakraborty, C. (2021) 'Early and accurate prediction of diabetics based on FCBF feature selection and SMOTE', *Int. J. Syst. Assur. Eng. Manag.*, pp.1–9.

18 Ohata, E.F., Bezerra, G.M., das Chagas, J.V.S., Neto, A.V.L., Albuquerque, A.B., de Albuquerque, V.H.C., Filho, P.P.R. (2020) 'Automatic detection of COVID-19 infection using chest X-ray images through transfer learning', *IEEE/CAA J. Autom. Sin.*, Vol. 8, No. 1, pp.239–248.

19 Padma, T. and Kumari, C.U. (2020) 'Deep learning based chest X-ray image as a diagnostic tool for COVID-19', *2020 International Conference on Smart Electronics and Communication (ICOSEC)*, Kongunadu College of Engineering and Technology, Tamil Nadu, India, pp.589–592.

20 Shi, F., Wang, J., Shi, J., Wu, Z., Wang, Q., Tang, Z., He, K., Shi, Y. and Shen, D. (2020) 'Review of artificial intelligence techniques in imaging data acquisition, segmentation and diagnosis for covid-19', *IEEE Rev. Biomed. Eng.*

21 Xie, Z., Wang, J., Zhao, C., Li, S., Gao, Y., Zhao, T. and Zhang, M. (2020) 'Imaging features of familial clustering of COVID-19', in *Diagnostic Imaging of Novel Coronavirus Pneumonia*, Springer, pp.163–207.

22 Farhat, H., Sakr, G.E. and Kilany, R. (2020) 'Deep learning applications in pulmonary medical imaging: recent updates and insights on COVID-19', *Mach. Vis. Appl.*, Vol. 31, No. 6, pp.1–42.

23 Kuchana, M., Srivastava, A., Das, R., Mathew, J., Mishra, A. and Khatter, K. (2020) 'AI aiding in diagnosing, tracking recovery of COVID-19 using deep learning on chest CT scans', *Multimed. Tools Appl.*, pp.1–15.

24 Pu, J., Leader, J.K., Bandos, A., Ke, S., Wang, J., Shi, J., Du, P., Guo, Y., Wenzel, S.E., Fuhrman, C.R., Wilson, D.O., Sciurba, F.C. and Jin, C.

25 Kishor, A., Chakraborty, C. and Jeberson, W. (2021) 'Reinforcement learning for medical information processing over heterogeneous networks', *Multimed. Tools Appl.*, pp.1–22.

26 Kishor, A., Chakraborty, C. and Jeberson, W. (2020) 'A novel fog computing approach for minimization of latency in healthcare using machine learning', *Int J. Interact Multimed Artif. Intell.*, Vol. 1, No. 1, pp.1–11.

27 Kishor, A., Chakraborty, C. and Jeberson, W. (2021) 'Intelligent healthcare data segregation using fog computing with internet of things and machine learning', *Int. J. Eng. Syst. Model. Simul.*, Vol. 12, Nos. 2–3, pp.188–194.

28 Küçükuğurlu, B. and Gedikli, E. (2020) 'Symbiotic organisms search algorithm for multilevel thresholding of images', *Expert Syst. Appl.*, Vol. 147, p.113210.

29 Kaveh, A. and Eslamlou, A.D. (2020) 'Water strider algorithm: a new metaheuristic and applications', *Structures*, Vol. 25, pp.520–541.

30 Rebouças Filho, P.P., da Silva Barros, A.C., Almeida, J.S.J., Rodrigues, P.C. and de Albuquerque, V.H.C. (2019) 'A new effective and powerful medical image segmentation algorithm based on optimum path snakes', *Appl. Soft Comput.*, Vol. 76, pp.649–670.

31 Pham, T.D. (2020) 'Classification of COVID-19 chest X-rays with deep learning: new models or fine tuning?', *Heal. Inf. Sci. Syst.*, Vol. 9, No. 1, pp.1–11.

32 Böger, B., Fachi, M.M., Vilhena, R.O., Cobre, A.F., Tonin, F.S. and Pontarolo, R. (2021) 'Systematic review with meta-analysis of the accuracy of diagnostic tests for COVID-19', *American Journal of Infection Control*, Vol. 49, No. 1, pp.21–29.

33 Xu, L., Jia, H., Lang, C., Peng, X. and Sun, K. (2019) 'A novel method for multilevel color image segmentation based on dragonfly algorithm and differential evolution', *IEEE Access*, Vol. 7, pp.19502–19538.

34 Al-Rahlawee, A.T.H. and Rahebi, J. (2021) 'Multilevel thresholding of images with improved Otsu thresholding by black widow optimization algorithm', *Multimedia Tools and Applications*, pp.1–27.

35 Albargathe, S.M.B.K., Kamberli, E., Kandemirli, F. and Rahebi, J. (2021) 'Blood vessel segmentation and extraction using H-minima method based on image processing techniques', *Multimed. Tools Appl.*, Vol. 80, No. 2, pp.2565–2582.

36 Alsarori, F.A., Kaya, H., Rahebi, J., Popescu, D.E. and Hemanth, D.J. (2020) 'Cancer cell detection through histological nuclei images applying the hybrid combination of artificial bee colony and particle swarm optimization algorithms', *Int. J. Comput. Intell. Syst.*, Vol. 13, No. 1, pp.1507–1516.

37 Masoud Abdulhamid, I.A., Sahiner, A. and Rahebi, J. (2020) 'New auxiliary function with properties in nonsmooth global optimization for melanoma skin cancer segmentation', *Biomed Res. Int.*, Vol. 2020, pp.1–14.

38 Abdullah, A.S., Rahebi, J., Özok, Y.E. and Aljanabi, M. (2020) 'A new and effective method for human retina optic disc segmentation with fuzzy clustering method based on active contour model', *Med. Biol. Eng. Comput.*, Vol. 58, No. 1, pp.25–37.